Molecular statics study of depth-dependent hysteresis in nano-scale adhesive elastic contacts

Weilin Deng and Haneesh Kesari ‡

School of Engineering, Brown University, Providence, RI 02912-0936, USA

E-mail: haneesh_kesari@brown.edu

March 2017

Abstract. The contact force–indentation-depth (P-h) measurements in adhesive contact experiments, such as atomic force microscopy, display hysteresis. In some cases, the amount of hysteretic energy loss is found to depend on the maximum indentation-depth. This depth-dependent hysteresis (DDH) is not explained by classical contact theories, such as JKR and DMT, and is often attributed to surface moisture, material viscoelasticity, and plasticity. We present molecular statics simulations that are devoid of these mechanisms, yet still capture DDH. In our simulations, DDH is due to a series of surface mechanical instabilities. Surface features, such as depressions or protrusions, can temporarily arrest the growth or recession of the contact area. With a sufficiently large change of indentation-depth, the contact area grows or recedes abruptly by a finite amount and dissipates energy. This is similar to the pull-in and pull-off instabilities in classical contact theories, except that in this case the number of instabilities depends on the roughness of the contact surface. Larger maximum indentation-depths result in more surface features participating in the load-unload process, resulting in larger hysteretic energy losses. This mechanism is similar to the one recently proposed by one of the authors using a continuum mechanics-based model. However, that model predicts that the hysteretic energy loss always increases with roughness, whereas experimentally it is found that the hysteretic energy loss initially increases but then later decreases with roughness. Our simulations capture this non-monotonic dependence of hysteretic energy loss on roughness.

PACS numbers: 81.07.Lk, 46.55.+d

Keywords: adhesive contact, hysteresis, surface roughness
Submitted to: *Modelling Simul. Mater. Sci. Eng.*

1. Introduction

Adhesive contacts play a central role in several important engineering applications and biological phenomena, such as friction [1–6], wear [7–9], stiction failure in

‡ Author to whom any correspondence should be addressed

MEMS [10, 11], cell adhesion [12], and gecko and insect locomotion [13, 14]. In particular, a clear understanding of adhesive contact processes and mechanics is critical for spatially mapping out a material's mechanical properties at the μm–nm length scales using techniques such as the atomic force microscopy (AFM) and nano-indentation (NI) [15–17]. The material properties are mapped by performing a set of contact experiments over a grid of points on the material's surface. The contact experiments often involve measuring the contact force, P, between the AFM or nanoindenter tip and the material substrate as a function of the indentation-depth, h, which is the maximum of the displacements the substrate's surface points undergo in the direction of the tip's motion. The material properties are then mapped by fitting the P-h curves measured at each location to an appropriate contact mechanics theory. At the μm–nm length scales surface forces, which include adhesive force arising due to van der Waals interactions, dominate, and are equally, if not more, important than the forces arising due to material mechanical deformations. Therefore the AFM and NI measured P-h curves are usually fitted to classical adhesive contact theories, such as the Johnson-Kendall-Roberts (JKR) [18], the Derjaguin-Muller-Toporov (DMT) [19], and the Maugis-Dugdale (MD) [20] theories.

The classical adhesive contact theories predict that once the solids are in contact (the region $h < 0$ in figure 1) the contact force between the solids depends only on the indentation-depth, irrespective of the history of the contact process (see figure 1 (a)). However, in many adhesive contact experiments [21–25] the contact force is observed to depend not only on the indentation-depth but also on whether the solids are moving towards ("loading phase") or away ("unloading phase") from one another (figure 1 (b)). And if the contact is in the unloading phase, then the contact force additionally depends on the maximum indentation-depth of the contact cycle. The maximum indentation-depth of a contact cycle, marked as $|h_{\min}|$ in figure 1 (b), is the indentation-depth at the beginning of the unloading phase in that contact cycle, which includes the loading and unloading phases. Thus, in experiments, the measured P-h curves from each contact cycle form a loop whose size depends on the $|h_{\min}|$ of that cycle. This depth-dependent hysteresis (DDH) phenomenon was often attributed to the formation of hydrogen bonds [22], meniscus related effects of ambient moisture [23], the entanglement and interdigitation of polymer chains [21, 26], and the inelastic material behaviors, such as viscoelasticity [27, 28] and plasticity [29, 30].

Kesari *et al.* [25, 31] reported an alternate, new mechanism for DDH in which DDH emerged as the smeared out effect of a series of small-scale surface imperfection created mechanical instabilities (SIMI) that take place at the growing and the receding edges of the contact interface. Their work is related to the works of Li and Kim [32] and Guduru [33]. Li and Kim [32] considered the adhesive contact problem between two solids, in which one of them was an elastic half-space and the other was a rigid solid with two-dimensional sinusoidal undulations on its surface. Guduru [33] considered the JKR-type adhesive contact between an elastic half-space and a rigid paraboloidal punch with superimposed sinusoidal undulations. Both works showed that the surface

undulations could create surface mechanical instabilities and consequently lead to an effective toughening of the contact interface. The mechanism through which small-scale roughness gives rise to DDH in the work of Kesari *et al.* [25, 31] is the same as the mechanism through which the undulations cause adhesive toughening in the work of Li and Kim [32] and Guduru [33].

Kesari *et al.* [25, 31] presented a continuum mechanics model for DDH. Using that model they argued that surface roughness features, such as depressions and protrusions, can temporarily arrest the contact area during both the loading and the unloading phase. And with a sufficiently large change of the indentation-depth, the arrested contact interface abruptly grows and recedes during the loading and the unloading phase, respectively, through the occurrence of energy dissipating surface mechanical instabilities. These instabilities are similar to the pull-in and pull-off instabilities seen in the classical adhesive elastic contact theories (figure 1 (a)), except that they occur at the length scale of surface roughness and can be numerous. The larger the $|h_{\min}|$, the more the number of the surface features that participate in the contact process, leading to the occurrence of a greater number of contact instabilities. Consequently, the energy loss, which is the cumulative energy lost at each of the instabilities, increases with $|h_{\min}|$, thus explaining the depth-dependence feature of DDH. The mechanism and model presented by Kesari *et al.* also captured a number of other experimentally observed features of DDH, such as (*eo.i*) the repeatability of the hysteresis loop on cyclically indenting the substrate to the same $|h_{\min}|$, (*eo.ii*) the force varying linearly with h during the initial stages of the unloading phase, (*eo.iii*) the loading branch of the P-h loop always falling on the same master curve, and (*eo.iv*) the unloading branch of the P-h loop converging to a master curve on sufficient unloading.

However, the surface instabilities postulated in the SIMI mechanism, to date, have not been directly observed in experiments. Furthermore, the model presented in [31] is based on many idealizations about the material's behavior and the topology of the contact region. For example, it assumes that the material is linear elastic and its deformation is infinitesimally small, the inter-body adhesive interactions are infinitesimally short ranged, and most importantly, the contact region is simply-connected. In view of these two points, it is natural to question whether the SIMI mechanism can indeed operate in real materials, in which due to surface asperities the contact region can be multiply-connected, and due to the highly localized nature of the surface tractions at any contacting asperities the asperities would have a high propensity to deform inelastically. Inelastic deformations are intrinsically dissipative process, and can, at least in theory, give rise to DDH.

We address this question by reporting here molecular-statics simulations of adhesive contact that show the SIMI mechanism in action. We carried out simulations of a quasi two-dimensional contact between a rigid tip and a deformable substrate in which the Dupré's work of adhesion [34] and the surface geometry were varied in a controlled manner. In the simulations, roughness is represented through surface's imperfections, such as pits and steps on the tip. Our simulations capture the primary features

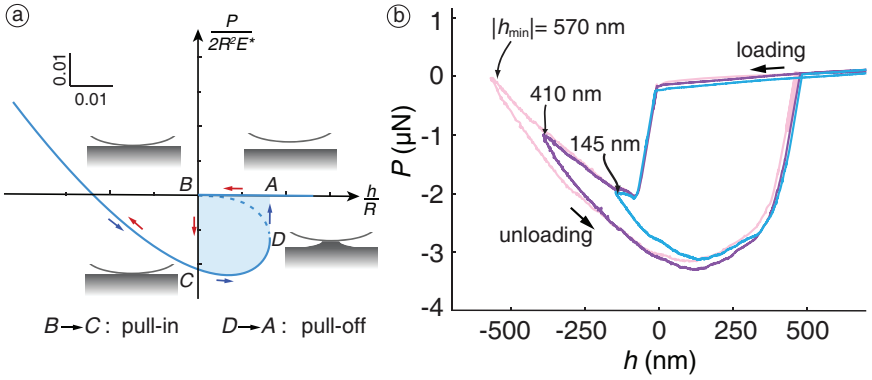

Figure 1. (color online) (a) The P-h curve as per the JKR theory. The pull-in ($B \to C$) and pull-off ($D \to A$) instabilities are marked along with the corresponding contact configurations. A contact cycle includes the loading and unloading phases. The shaded area, i.e., the size of the hysteresis loop formed in a contact cycle due to the instabilities, is depth independent. (b) The P-h curves measured in the glass bead-Poly(dimethylsiloxane) (PDMS) contact experiment. The size of the hysteresis loop depends on the maximum indentation-depth $|h_{\min}|$. See [25] for the details of the contact experiment.

of the SIMI mechanism reported in [25, 31]. However, the primary significance of our simulations is that they demonstrate that the SIMI mechanism can operate at conditions that are much more general than those assumed in [31]. For example, in our simulations the contact region is multiply-connected with the contact tractions being highly localized at the surface imperfections, the inter-body forces have a finite range, and the material model—Stillinger-Weber (SW) potential for silicon [35]—is fairly general, since it allows for the free operation of various inelastic mechanisms, such as plasticity, phase transformations, and the creation and motion of dislocations. Thus, our simulations provide critical support to the SIMI mechanism as a viable explanation for DDH in real materials.

2. Simulation model and method

In our molecular-statics simulation, we consider a quasi two-dimensional contact between a rigid tip and a deformable substrate. The tip is created by sculpting and/or deforming a slab of perfect Si crystal. To investigate the effect of surface roughness on adhesive contact, we create tips with various model surface profiles, such as the smooth-wedge tip, the pitted-wedge tip, the parabolic tip, and the stepped tip (see figures 2 (a)–(d), respectively). Atoms in the tip are initially arranged to have perfect lattice structure of crystalline silicon, with the [100], [010], and [001] crystal orientations being in the x, y, and z directions, respectively. And their relative positions are rigidly fixed through out the simulation to facilitate the introduction of the above mentioned surface features. The substrate is a single crystal of Si with dimensions 815 Å, 272 Å, and 10 Å in x, y and z directions, respectively, which has the same crystal orientation as the tip.

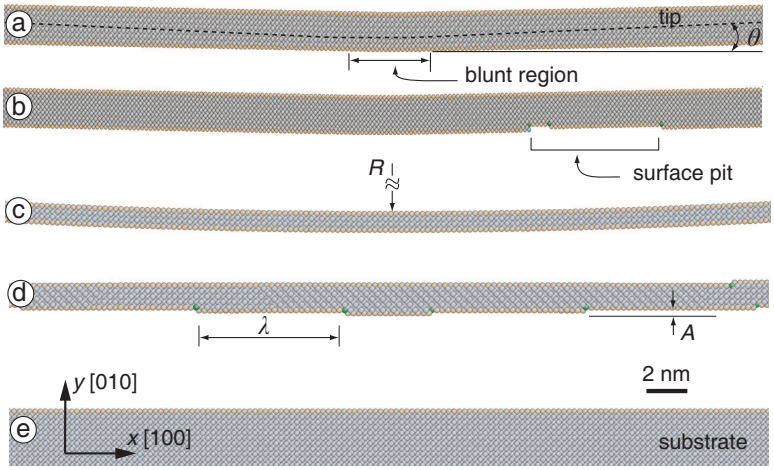

Figure 2. (color online) The tips and substrate used in the simulations. The colors denote the atomic coordination number, with gray-4, green-3, and gold-2. (a) Smooth-wedge tip. The tip has three atomically smooth facets; the right and the left facets are at an inclination of $\theta \approx \pm 1^\circ$ to the substrate's surface, respectively, while the middle one is parallel to it. The blunt region is of width 2 nm. (b) Pitted-wedge tip. This tip is the same as the smooth-wedge tip except for that a surface pit of width 9 nm and depth 5 Å, has been carved into its right facet. (c) Parabolic, atomically smooth, tip. The tip has a curvature of $1/R = 150$ nm^{-1} at its vertex. (d) Stepped tip with steps of length $\lambda = 8.7$ nm and height $A = 1.36$ Å. We use stepped tips of different λ and A in our simulations. (e) shows the substrate along with the x and y coordinate directions. The scale bar of 2 nm applies to all subfigures.

Periodic boundary conditions are applied in the x and z directions. The bottom eight atomic planes of the substrate are held fixed during the simulations. The interactions among atoms in the substrate are modeled by the SW potential of Si [35]. And the interaction between the substrate and the tip are modeled by the Lennard-Jones (LJ) potential [36] $V(r) = 4\epsilon\left[(\sigma/r)^{12} - (\sigma/r)^6\right]$, where ϵ is the depth of the potential well, σ is the distance at which the potential is zero, and r is the interatomic distance. For the purpose of computational efficiency, each potential has a cut-off following the method in [37], with a maximum range of 3.8 Å for SW and 2.8 Å for LJ. In our simulations, the Dupré's work of adhesion, w, is equal to $1.537\epsilon n^2\sigma^4$, where $n = 5 \times 10^{28}\,\mathrm{m}^{-3}$ is the atomic density of Si. We set $\sigma = 2.095$ Å and vary ϵ to modulate w. Unless stated otherwise, we use $\epsilon = 0.521$ eV, which corresponds to $w = 618\,\mathrm{mJ/m^2}$.

At the beginning of each simulation the tip is positioned such that there is no interaction between the tip and the substrate atoms. In our simulations, the indentation-depth, h, is the distance traveled by the tip in the y direction. The datum for h is chosen such that $h = \sigma$ when the tip and the substrate just start interacting. The tip is moved towards the substrate in the $-y$ direction until h equals a pre-assigned value, $|h_{\min}|$, and then retracted back until the tip-substrate contact force vanishes. The tip's motion is controlled in steps of 0.01 Å. Each step is followed by a relaxation of the potential energy to a local minimum using the conjugate-gradient algorithm [38]. To obtain the P-h curve in the simulation, we compute the net tip-substrate contact force in the y

direction after each relaxation by summing up the forces acting on all the tip atoms.

3. Results and discussions

Figure 3 (a) shows the P-h curve (thick curve) from a contact simulation involving the smooth-wedge tip shown in figure 2 (a) and the substrate shown in figure 2 (e). The P-h curve exhibits a single and repeatable hysteresis loop, caused by the initial pull-in and the final pull-off instabilities predicted by the classical adhesive elastic contact theories. The energy loss due to the classical pull-in and pull-off instabilities is a characteristic phenomenon during adhesive elastic contact of any tip having a smooth monotone profile. Though this hysteresis loop is repeatable on cyclic loading, it is qualitatively different from DDH since its size does not depend on $|h_{\min}|$.

Next, we perform the same simulation but with the pitted-wedge tip (figure 2 (b)). The pitted-wedge tip was created by removing a thin strip of atoms from the surface of the wedge tip. Interestingly, this leads to another hysteresis loop in figure 3 (a) (thin curve). At the end of the first load-unload cycle, the atomic displacements with respect to the initial positions are negligible and the P-h curve for the second cycle essentially overlaps with the first one. It is easy to see that the additional hysteresis loop would not appear if $|h_{\min}|$ was less than 1 Å. This proves, in principle, that DDH can exist without any plasticity, even though the shape of the hysteresis loop is still somewhat different from that observed in experiments (e.g., see figure 1 (b)).

The underlying mechanism responsible for the additional hysteresis appearing for the pitted-wedge tip but not for the smooth-wedge tip can be seen in action by visualizing the configurations during a load-unload cycle. Some representative snapshots of the configurations during a load-unload cycle of the pitted-wedge tip are shown in figure 3 (b)–(e). For the smooth-wedge tip simulation, after the classical pull-in instability (at $h \approx -0.4$ Å), the contact width grows continuously with increasing indentation-depth. On the other hand, after the classical pull-in instability, the small surface pit on the pitted-wedge tip is able to arrest the contact width, all the way until h reaches -2.6 Å (figure 3 (b)). This is because the tip atoms in the surface pit are outside the interaction range of the substrate atoms. With a slight further increase of $|h|$ contact is suddenly established in an area beyond the surface pit (figure 3 (c)). Upon unloading, the newly formed contact area persists until $h \approx -1.2$ Å (figure 3 (d)). Therefore, in the range of -2.6 Å $< h < -1.2$ Å, the contact area is different during the loading and unloading phases, giving rise to the additional hysteresis loop. It is interesting to note that in this range the contact area is multiply-connected, which is in contrast with the simply-connected contact region assumption made in [31].

It is known that a real surface is usually rough containing many imperfections such as depressions and protrusions. To model the effect of surface roughness on adhesive contact, we simulate the contact between the substrate and the stepped tip shown in figure 2 (d). In the tip, each step has height A and neighboring steps are separated by λ from each other. Figures. 4 and 5 show the P-h curves from the contact simulations

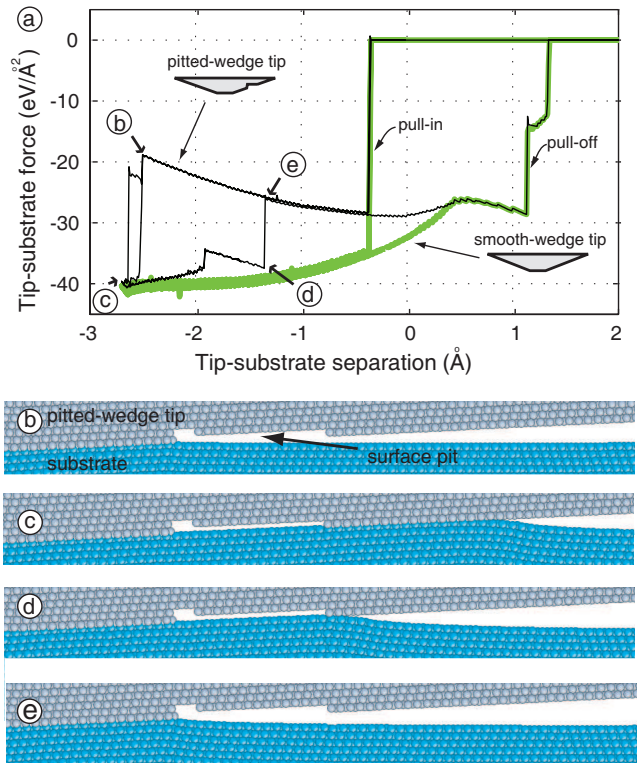

Figure 3. (color online) (a) The P-h curves from simulations employing the smooth-wedge tip (thick curve) and the pitted-wedge tip (thin curve). (b)–(e) Tip-substrate configurations at different instances of the pitted-wedge tip simulation. The simulation instances corresponding to those configurations are marked on the P-h curve in (a) using labels ⓑ–ⓔ.

involving the stepped tip. The P-h curves for the small adhesion value of $w = 35$ mJ/m^2 (figure 4 (a), thick solid curve) show five small hysteresis loops. The very first loop, when counting from right to left, corresponds to the classical pull-in and pull-off contact instabilities. By studying the evolution of the tip-substrate configurations during the simulation we found that each of the remaining loops correspond to the unstable contact growth and recession across an edge belonging to the tip's surface steps. We saw that during the loading phase the contact area got arrested at each of the step edges and then only grew when further loading brought the region ahead of the steps unstably into contact. And during the unloading phase as the contact region receded and approached a step edge, a patch of the contact region ahead of the step edge detached unstably. Thus, the second and the third loops correspond to unstable contact growth and recession across the bottom most step's two edges, one on the left and the other on the right§. And the last two loops correspond to the edges of the left and right steps that are immediately above the bottom most step. So, the mechanism of unstable contact growth and recession across a surface imperfection previously seen

§ In our simulation the contact process was asymmetric between the left and the right sides of the tip. This is in contrast with what is assumed in classical adhesive contact theories.

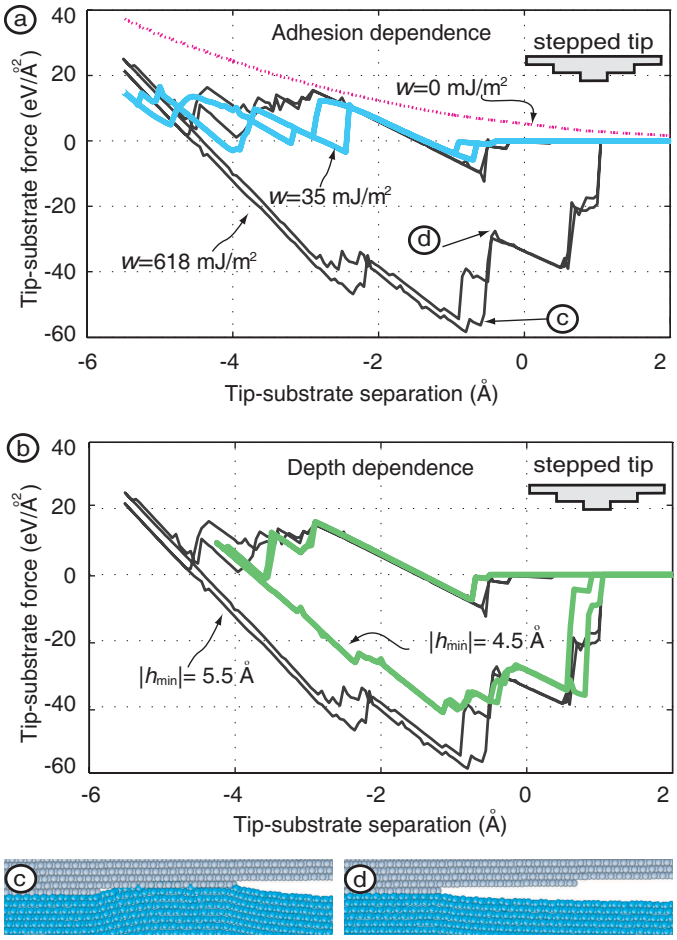

Figure 4. (color online) (a) The P-h curves show the effect of w in the stepped tip simulations. For $w = 35$ mJ/m^2, each step induces a hysteresis loop, and these coalesce with one another upon increasing w to 618 mJ/m^2. When $w = 0$, no hysteresis is observed. (b) The P-h curves from simulations employing the stepped tip. These curves display repeatable hysteresis loops, whose size increases with $|h_{\min}|$. (c)–(d) Tip-substrate configurations at different instances of the stepped tip simulation. The simulation instances corresponding to those configurations are marked on the P-h curve in (a) using labels ⓒ–ⓓ.

in the pitted-wedge simulation operates here as well, and more importantly, it operates repeatedly at each imperfection.

The events of unstable contact growth and recession across surface imperfections are in some ways similar to the classical pull-in and pull-off contact instabilities. However, there are two important differences between the two. First, the newly observed contact instabilities occur at the length scale of the surface imperfections, whereas the classical pull-in and pull-off instabilities occur at a much larger length scale. For example, as per the JKR theory, after the pull-in instability the radius of the contact patch formed is equal to $(2\pi R^2 w/E^*)^{1/3}$, where $1/R = (1/R_1 + 1/R_2)$, R_1 and R_2 are, respectively, the radii of mean curvatures of the contacting solids' surfaces at the points where they first make contact, $1/E^* = (1-\nu_1^2)/E_1 + (1-\nu_2^2)/E_2$, and E_i and ν_i $(i = 1, 2)$ are the

Young's moduli and Poisson's ratios of the contacting solids. Using this estimate we get the radius of the initial contact patch in the AFM experiments reported in [25] to be about 5 μm. Whereas the AFM tip in [25] is reported to have a Root Mean Square (RMS) roughness of about 6 nm and the molds on which the PDMS substrates were cast are reported to have RMS roughnesses ranging from 0.65 to 1.52 nm. Second, in any contact cycle there is always only a single pair of the classical pull-in and pull-off instabilities, and the size of the hysteresis loop it generates is independent of $|h_{\min}|$ (figure 1 (a)). Whereas the surface imperfection level instabilities can be numerous, and as we first described using the pitted-wedge tip simulation, the number of such instabilities depend on $|h_{\min}|$. This, in fact, is the precise mechanism through which the surface imperfection level instabilities give rise to the depth-dependence aspect of DDH in the SIMI mechanism. The total energy loss in a contact cycle is the cumulative energy lost during all the contact instabilities, both at the large- (classical pull-in and pull-off) and small-scale (surface imperfection level). The size of the DDH loop represents the net energy loss in a contact cycle, therefore, when the surface imperfection level instabilities are active the DDH loop's size will naturally grow with $|h_{\min}|$.

The simulations also reveal that the surface imperfection instabilities—and consequently the DDH they give rise to—are primarily governed by surface adhesion and roughness. For example, despite the surface steps the surface imperfection level instabilities, and consequently their corresponding hysteresis loops, vanish when there is no adhesion between the tip and the substrate, i.e., when $w = 0$ (figure 4 (a), dashed curve). We modulated w by adjusting the LJ potential parameter ϵ. At large adhesion, e.g., $w = 618$ mJ/m^2 (figure 4 (a), thin solid curve), the loops corresponding to the different surface imperfections merge to form one large hysteresis loop whose size depends on $|h_{\min}|$ (see figure 4 (b)). This loop has a tapered shape that resembles the DDH loops seen in experiments (cf. figure 1 (b) and figure 4 (b)). In fact, the P-h curves from these simulations also capture the experimentally observed DDH features *eo.i-iv.* Despite the individual hysteresis loops no longer being clearly discernible, the surface imperfection level instabilities, with which we identified each of the individual loops in the small adhesion, $w = 35$ mJ/m^2 simulation (figure 4 (a), thick solid curve), however, are still very much active. For example, the tip-substrate configurations before and after the occurrence of a contact recession instability in the $w = 618$ mJ/m^2 simulation are shown in figures 4 (c) and (d), respectively. This instability occurs during the unloading phase and across the lower most step's right edge. The abrupt contact force increase corresponding to this instability is marked in figure 4 (a) using labels (c) and (d).

However, adhesion alone is insufficient for the creation of DDH. For example, figure 5 (a) shows the P-h curves from two large adhesion, $w = 618$ mJ/m^2, simulations, in which $|h_{\min}| = 2$ and 5 Å, respectively. As can be seen, these P-h curves do not display any DDH. The reason for this is that the tip employed in these simulations is the atomically smooth, parabolic tip shown in figure 2 (c). Therefore, both adhesion and roughness are critically necessary for the creation of DDH through the SIMI mechanism.

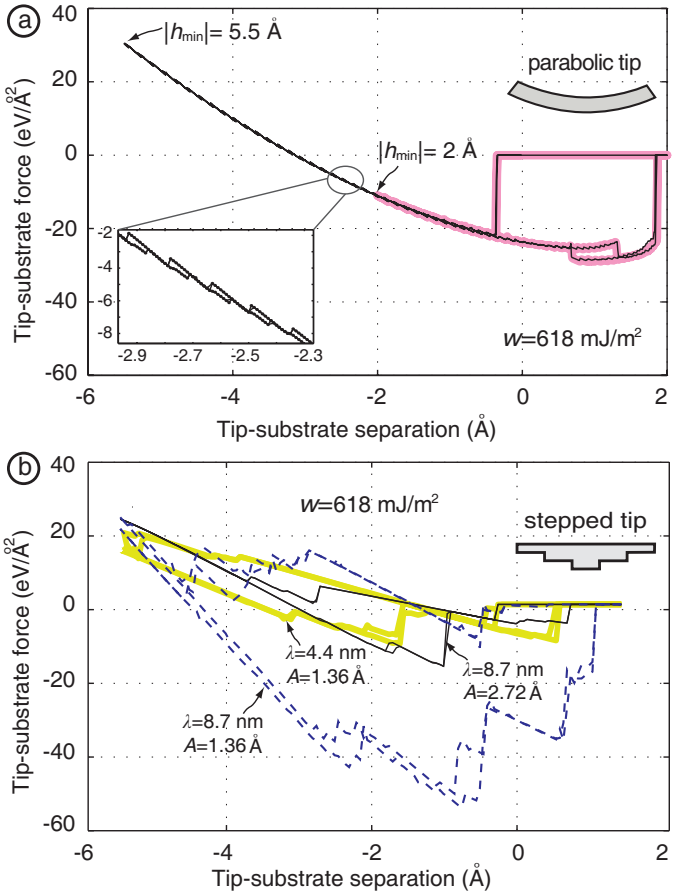

Figure 5. (color online) (a) The P-h curves from simulations employing the parabolic tip and displaying only depth-independent hysteresis. Inset: Small disconnected loops due to the abrupt bond formation and breakage between the tip and the substrate atoms. (b) The P-h curves from simulations employing stepped tips of different step lengths and heights.

In our simulations we found the DDH energy loss, for a given $|h_{\min}|$, to always increase with w, see, e.g., figure 4 (a). This observation is consistent with the theory presented in [25, 31]. We do not quantitatively compare our simulation results with the theory presented in [25, 31], since that theory applies to axisymmetric contact in which the substrate in an isotropic half-space, whereas the contact in our simulations is quasi two-dimensional and the substrate in them is neither isotropic nor a half-space. Furthermore, in the theory presented in [25, 31] the contact region is assumed to be always simply-connected, whereas in all our simulations involving model imperfections the contact region is multiply-connected (see figures 3 (b)–(e) and figures 4 (c)–(d)).

The dependence of DDH on roughness is much more interesting. The P-h curve (thin curve) shown in figure 5 (a) for the parabolic tip can directly be compared with the P-h curve (thin curve) shown in figure 4 (b) for the stepped tip, since both of them correspond to $|h_{\min}| = 5.5\,\text{Å}$ and $w = 618\ \text{mJ/m}^2$. From the comparison we can see that adding surface imperfections increases the energy loss in a contact cycle. As already

explained, the additional energy loss is due to the new surface instabilities created by the added imperfections. Figure 5 (b) shows additional P-h curves from the stepped tip simulations in all of which $|h_{\min}| = 5.5$ Å and $w = 618$ mJ/m^2. However, A and λ vary between the simulations. From those curves we can see that the hysteretic energy loss increases from 56.88 to 198 eV/ Å on increasing λ from 4.4 to 8.7 nm, and decreases from 198 to 33.84 eV/ Å on increasing A from 1.36 to 2.72 Å. In our simulations, we use the parameter A^2/λ as a measure of surface roughness (see the online supplementary data for the discussion). Thus, the curves shown in figure 5 (b) demonstrate that the hysteretic energy loss eventually decreases on increasing roughness. Therefore, it is found from figures 5 (a) and (b) that the DDH energy loss initially increases and then later decreases with roughness. This observation is consistent with the experimental findings reported in [1, 25]. In contrast, the theory presented in [25, 31] predicts that the hysteretic energy loss will always increase with roughness. As stated in [25, 31], the prediction of energy loss always increasing with roughness is a consequence of the assumption in [25,31] that the contact region is always simply-connected. Therefore, the theory presented in [31] is a good model for DDH only when the roughness is sufficiently small, so that it is reasonable to assume a simply-connected contact region, and it does not apply when the roughness is large so that the contact region is more likely to be multiply-connected, as is the case in our simulations. Hence, we believe that there is a need for a more comprehensive theory of DDH, one that describes DDH both at small and large roughnesses.

The inelastic deformations such as viscoelasticity [27, 28] and plasticity [29, 30] can give rise to DDH. However, the DDH we report in our simulations is not due to any of such mechanisms. Viscoelasticity can be readily ruled out as contributing to DDH in our simulations since we perform the simulations in a quasi-static manner. The fact that the DDH in our simulations is not due to plasticity can most clearly be seen from the P-h curves. All the P-h curves we report (figures. 3–5) are from two consecutive load-unload cycles. As can be seen in the figures, the P-h curve from the second cycle closely follows the one from the first. This would not be possible if there was plasticity in the simulations. There are, however, some small differences between the P-h curves from the first and the second cycle. These differences are due to the reconstruction of the substrate's surface atoms during the contact simulation. This is because, we found that the small differences become almost imperceptible if we relax the substrate, by annealing it using molecular dynamics simulations and then quenching it using conjugate gradient energy minimization, before beginning the contact simulations (see the online supplementary data, figure 2). We also checked for plasticity by monitoring the strain and the co-ordination number of the atoms in the substrate during the simulations. Such checks also helped us to rule out additional inelastic mechanisms, such as phase transformations, and also simulation artifacts, such as surface amorphization, and interpenetration of the tip and substrate atoms.

4. Concluding remarks

We conclude by noting that the mechanism for DDH proposed by Israelachvil *et al.* [26], termed mechanical hysteresis, is similar to the SIMI mechanism presented in [25,31] and this work. The similarity lies in the fact that in both mechanisms DDH is the cumulative effect of many individual hysteretic events. In the mechanical hysteresis mechanism the individual hysteretic events are the unstable bond formation and breakage between the atoms of the tip and the substrate. In the SIMI mechanism the individual hysteretic events are the unstable contact growth and recession across the surface imperfections, which occur at the length scale of surface roughness. The instabilities in the SIMI mechanism operate at a much larger length scale compared those in the mechanical hysteresis mechanism, and consequently the DDH energy loss in the SIMI mechanism is much larger. Some of our simulations, such as the ones involving the parabolic tip (figure 5 (a)), also capture the mechanical hysteresis mechanism. A closer examination of the P-h curves from the parabolic tip simulations show that the seemingly single valued P-h curve, in the region $h < 0$, actually consists of many small, disconnected, hysteresis loops. On visualizing the simulations we found the small disconnected loops to be due to abrupt bond formation and breakage between the tip and the substrate atoms, i.e., due to the mechanical hysteresis mechanism. However, the energy loss of the disconnected loops is only about 0.029 eV/ Å, which is only 0.0146% of that results from the SIMI mechanism. Therefore, the energy loss due to the mechanical hysteresis mechanism in our simulations is negligible compared to the energy loss due to the SIMI mechanism.

Acknowledgments

This work is partly supported by the NSF grant CMMI-1562656. Weilin Deng is partially supported by a graduate fellowship from the China Scholarship Council.

References

[1] Briggs G and Briscoe B 1976 *Nature* **260** 313–315
[2] She H, Malotky D and Chaudhury M 1998 *Langmuir* **14** 3090–3100
[3] Urbakh M, Klafter J, Gourdon D and Israelachvili J 2004 *Nature* **430** 525–528
[4] Maeda N, Chen N, Tirrell M and Israelachvili J 2002 *Science* **297** 379–382
[5] Li Q and Kim K S 2008 *Proc. R. Soc. A* **464** 1319–1343
[6] Hulikal S, Bhattacharya K and Lapusta N 2015 *Journal of the Mechanics and Physics of Solids* **76** 144–161
[7] Bhushan B, Israelachvili J N and Landman U 1995 *Nature* **374** 607–616
[8] Jacobs T D and Carpick R W 2013 *Nature nanotechnology* **8** 108–112
[9] Aghababaei R, Warner D H and Molinari J F 2016 *Nature communications* **7**
[10] DelRio F W, de Boer M P, Knapp J A, Reedy E D, Clews P J and Dunn M L 2005 *Nature materials* **4** 629–634
[11] Maboudian R and Howe R T 1997 *Journal of Vacuum Science & Technology B* **15** 1–20
[12] Chu Y S, Dufour S, Thiery J P, Perez E and Pincet F 2005 *Physical Review Letters* **94** 028102

[13] Autumn K, Liang Y A, Hsieh S T, Zesch W, Chan W P, Kenny T W, Fearing R and Full R J 2000 *Nature* **405** 681–685
[14] Song Y, Dai Z, Wang Z, Ji A and Gorb S N 2016 *Scientific Reports* **6**
[15] Sun Y, Akhremitchev B and Walker G C 2004 *Langmuir* **20** 5837–5845
[16] Ebenstein D M and Pruitt L A 2006 *Nano Today* **1** 26–33
[17] Cross S E, Jin Y S, Tondre J, Wong R, Rao J and Gimzewski J K 2008 *Nanotechnology* **19** 384003
[18] Johnson K, Kendall K and Roberts A 1971 *Proc. R. Soc. A* **324** 301–313
[19] Derjaguin B V, Muller V M and Toporov Y P 1975 *Journal of Colloid and Interface Science* **53** 314–326
[20] Maugis D 1992 *Journal of Colloid and Interface Science* **150** 243–269
[21] Choi G, Kim S and Ulman A 1997 *Languir* **13** 6333–6338
[22] Silberzan P, Perutz S, Kramer E J and Chaudhury M K 1994 *Langmuir* **10** 2466–2470
[23] Pickering J, Van Der Meer D and Vancso G 2001 *Journal of Adhesion Science and Technology* **15** 1429–1441
[24] Guduru P and Bull C 2007 *Journal of the Mechanics and Physics of Solids* **55** 473–488
[25] Kesari H, Doll J C, Pruitt B L, Cai W and Lew A J 2010 *Philosophical Magazine Letters* **90** 891–902
[26] Chen Y, Helm C and Israelachvili J 1991 *Journal of Physical Chemistry* **95** 10736–10746
[27] Tirrell M 1996 *Langmuir* **12** 4548–4551
[28] Giri M, Bousfield D B and Unertl W 2001 *Langmuir* **17** 2973–2981
[29] Landman U, Luedtke W, Burnham N and Colton R 1990 *Science* **248** 454–461
[30] Landman U, Luedtke W and Ringer E M 1992 *Wear* **153** 3–30
[31] Kesari H and Lew A J 2011 *Journal of the Mechanics and Physics of Solids* **59** 2488–2510
[32] Li Q and Kim K S 2009 *Acta Mechanica Solida Sinica* **22** 377–390
[33] Guduru P 2007 *Journal of the Mechanics and Physics of Solids* **55** 445–472
[34] Maugis D 2000 *Contact Adhesion and Rupture of Elastic Solids* Solid State Sciences (Springer)
[35] Stillinger F H and Weber T A 1985 *Physical Review B* **31** 5262
[36] Israelachvili J N 1985 *Intermolecular and Surface Forces* (Academic press)
[37] Plimpton S 2008 *LAMMPS User's Manual*
[38] Ruszczynski A 2011 *Nonlinear optimization* (Princeton University Press)